

# Mechanistic Model for the Prediction of Top-of-the-Line Corrosion Risk

F. Vitse,<sup>‡\*</sup> S. Nešić,<sup>\* Y.</sup> Gunaltun,<sup>\*\* D.</sup> Larrey de Torreben,<sup>\*\*</sup> and P. Duchet-Suchaux<sup>\*\*</sup>

## ABSTRACT

A model is presented for the prediction of the corrosion rate by carbon dioxide (CO<sub>2</sub>) under dewing conditions. A mechanistic approach is developed that takes into consideration the hydrodynamics, thermodynamics, heat and mass transfer, chemistry, and electrochemistry during the phenomenon of top-of-the line corrosion. This model is validated by experimental data. It offers a better insight into the role played by primary parameters such as temperature, total pressure, partial pressure of CO<sub>2</sub>, gas velocity, and condensation rate.

**KEY WORDS:** carbon dioxide corrosion modeling, condensation rate, corrosion rate, noncondensable gas, protective scale, scaling tendency, top-of-the line corrosion

## INTRODUCTION

In the case where a pipeline cannot be protected from internal corrosion by the injection of corrosion inhibitors, a reliable control device and some accurate predictive tools of the corrosion rate are required. In the specific case of top-of-the-line corrosion (TLC), the stratified or stratified-wavy flow regime does not provide good wettability by inhibitors<sup>1</sup> of the upper part of the internal pipewall.

Noninhibited water is present at the top of the line due to the condensation of water vapor transported along the pipe with other gases. As important heat exchanges take place between the pipe and its surrounding, a certain amount of water will condense at the pipewall leading to a corrosive environment.<sup>2</sup> To qualitatively and quantitatively describe the phenomena of corrosion occurring at the top of the line, a deep insight into the combined effect of the chemistry, hydrodynamics, thermodynamics, and heat and mass transfer in the condensed water is needed.<sup>3</sup>

In this paper, the corrosion rate in the presence of carbon dioxide (CO<sub>2</sub>) was studied experimentally along with the condensation rate of water in a horizontal pipeline in the presence of a noncondensable gas. Particular attention was given to the following parameters: temperature of the gas bulk, temperature of the pipewall, total pressure in the system, partial pressure of CO<sub>2</sub> (P<sub>CO<sub>2</sub></sub>), gas velocity, and condensation rate.

A mechanistic model was developed that gives a better insight into the role played by the aforementioned parameters. The model was tuned on a large set of experimental data offering a convenient predictive tool for the risk of top-of-the-line corrosion (TLC) by CO<sub>2</sub>. This model can be used directly to optimize the design of pipelines since it allows the determination of the level of thermal insulation required to avoid the condensing conditions leading to an unacceptable rate of corrosion.

Submitted for publication February 2003; in revised form, June 2003.

<sup>‡</sup> Corresponding author.

\* Corrosion in Multiphase Systems Center, Institute for Corrosion and Multiphase Technology, Ohio University, Athens, OH 45701.

\*\* Exploration and Production TotalFinaElf, 92069 Paris La Defense.

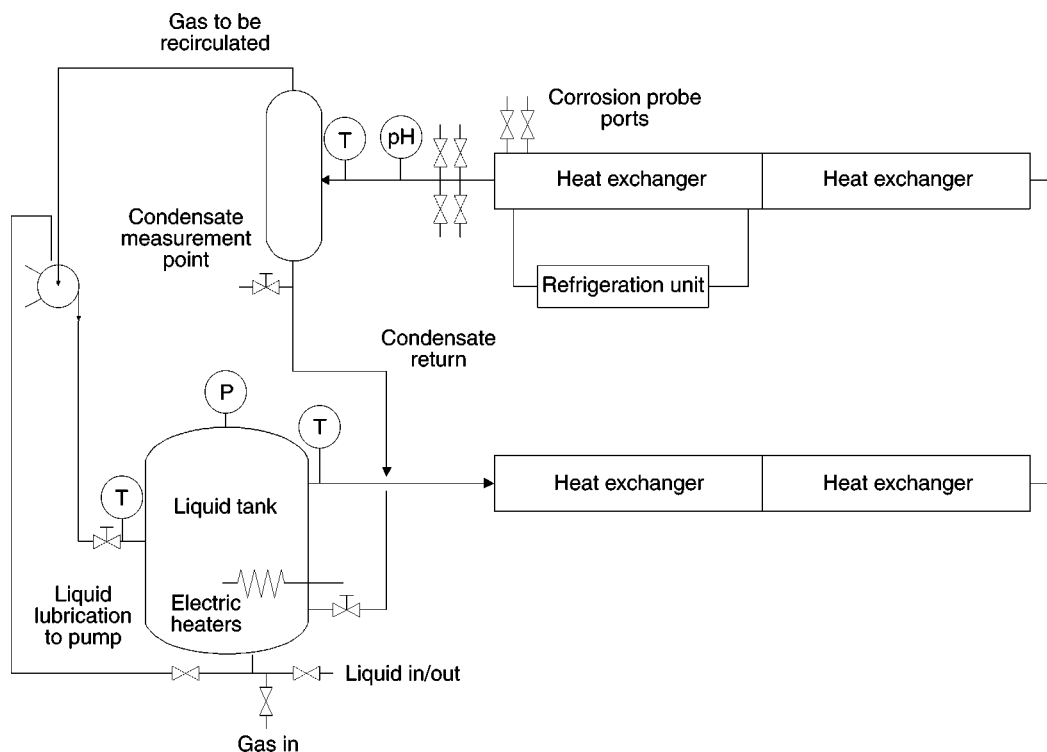


FIGURE 1. Schematic of the flow loop.

## EXPERIMENTAL PROCEDURES

### Experimental Setup and Procedure

To reproduce the conditions encountered in the field during the production of wet gas, a full-scale flow loop was built in our laboratories. The schematic of the loop is given in Figure 1. The experimental procedure is as follows: CO<sub>2</sub> was injected first in the flow loop up to a specific pressure. In a 1-m<sup>3</sup> stainless steel (SS) tank, water was then heated by electrical heaters up to the temperature of interest. The total pressure was recorded. The pump was then started and the mixture of CO<sub>2</sub> and water vapor flowed in the 4-in. SS loop until steady-state conditions were reached in the gas phase inside the pipe. A counter-current double-pipe heat exchanger was used to cool the gas mixture and control the condensation rate. The coolant used for this specific application was water. The condensed water was collected in a pressure vessel; this configuration allows sampling without disturbing the flow and the pressure in the loop. The measured condensation rate was equal to the amount of water condensed in the heat exchanger divided by its surface area and by the time of experimentation.

The real-time measurement of the corrosion rate starts once a steady state was attained. Data acquisition devices are set to continuously measure the inlet

and outlet temperature of the gas bulk, the inside wall temperature at a position close to where the corrosion probe is installed, the total pressure, the gas velocity, the temperature at the inlet and outlet of the cooling liquid, the cooling liquid flow rate, and the corrosion rate. Figure 2 shows the design of the heat exchanger, the insertion ports for the flush-mounted probes, and the position of the data acquisition for temperatures and flow rates. The temperature of the probe head was also continuously monitored using the Ceion<sup>†</sup> technology (resolution: ±0.5°C): the probe head is made of two identical sensing elements with the shape of two concentric spirals. One of the spirals, coated by a thin layer of epoxy, is immune to corrosion and serves both purposes of temperature compensation and temperature monitoring. Since both elements are physically very close and subject to the same external conditions, it can be assumed that they have the same temperature. Therefore, the temperature of the corroding element was known and could be set identical to the surrounding wall temperature by an air-cooling system built within the probe body.

### Setup and Data Acquisition for Corrosion Measurement

During TLC, it is particularly important to know the local wall temperature on the inner pipewall in addition to the bulk gas temperature. There are two reasons for this:

<sup>†</sup> Trade name.

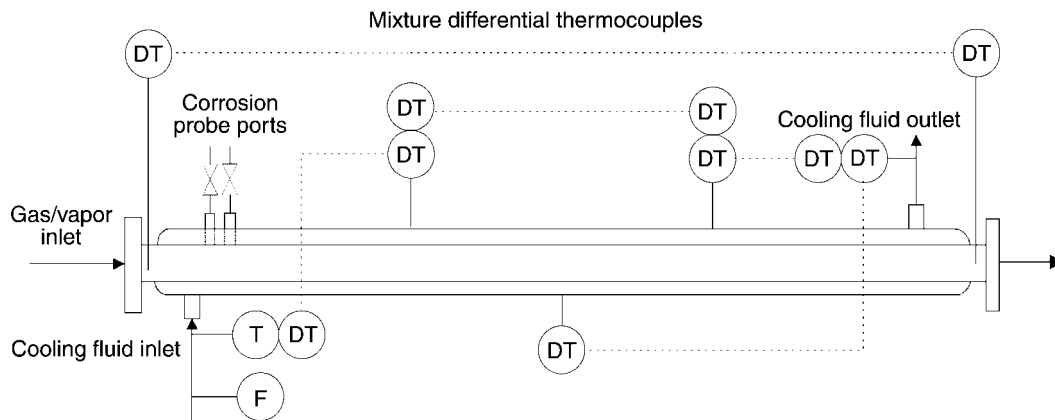


FIGURE 2. Double-pipe counter-current heat exchanger design.

- Because the fluid transported is gas, and because significant heat exchanges occur at the wall, an important temperature gradient can occur between the bulk phase and the wall. In such a case, the wall temperature is more adapted than the bulk temperature to predict the kinetics of the electrochemical reaction of corrosion.
- The condensation rate of water vapor will be dependent on the heat and mass transfer in the gas phase. These transfers are related to the gradient of temperature occurring between the gas bulk and the pipewall. Thus, an accurate measurement and control of the wall temperature is needed to set the local condensation rate.

For these reasons, the probe used for the measurement of the corrosion rate must be kept at the same temperature as the rest of the wall. A new technology of “air-cooled” corrosion probe is used and validated for this specific project. By allowing a flow of air through the body of the probe, the temperature of the sensing element can be kept identical to the wall temperature. A data acquisition system linked to a thermosensor in the probe head allows such monitoring.

The electrical resistance (ER) measurement technique is used during experimentation on TLC. The air-cooled probe used for this specific application had a 1-mm-thick sensor; the resolution for such a thickness was 5 nanometers.<sup>4</sup> Electrochemical techniques were avoided for several reasons: the conductivity of condensed water may be too low to give a reasonable reading. Also, at low condensation rates, the condensed water film on the probe head may not be continuous, preventing the current from flowing between the working and the counter electrodes.

Some additional coupon weight loss measurements (CWL) were run simultaneously to ER to validate the experimental results. For CWL measurements, the same type probe body (air-cooled) was

used. For each experiment, the measurement obtained with CWL was within  $\pm 40\%$  of the corresponding ER measurement.

## RESULTS

In some cases, the effect of some primary parameters on the condensation rate and on the corrosion rate could be isolated by keeping the other parameters of experimentation as constants. In other cases, the parameters of interest were coupled and so is their effect on the corrosion and condensation rates. All the following tests were run over a period of time from 48 h to 120 h. For each test, the corrosion rate reported was the stabilized rate (the corrosion rate was considered stable when no change  $>0.05$  mm/y occurred during a period of time of at least 12 h). For each experiment, which was repeated many times, the error bar shown in Figures 3 through 5 represents the standard error. However, some experiments were not reproduced. For these experiments, the error bars reported correspond to the standard error as calculated for the experiment:  $T = 50^\circ\text{C}$ ,  $P_{\text{CO}_2} = 4$  bar, gas velocity = 4 m/s, high cooling. These error bars are given as a support of the quantitative description of the phenomena observed and to validate the quantitative conclusions that are drawn.

### *Influence of the Bulk Temperature and the Wall Temperature on the Corrosion Rate*

The influence of temperature was studied over a range from  $40^\circ\text{C}$  to  $100^\circ\text{C}$ . First, as the temperature increased up to  $70^\circ\text{C}$  to  $80^\circ\text{C}$ , the corrosion rate increased as well. Then, the trend is reversed and the corrosion rate decreases as the temperature increases to  $90^\circ\text{C}$ . The condensation rate, however, keeps increasing as the temperature increases (Figure 5). As can be seen from Figure 3, the same trend showing a maximum corrosion rate between  $70^\circ\text{C}$  and  $80^\circ\text{C}$  was observed depending on the  $\text{CO}_2$  partial pressure.

**Notations:**

In what follows:

\*Normalized corrosion rate =

$$\frac{\text{corrosion rate}}{\text{maximum experimental corrosion rate}}$$

\*Normalized condensation rate =

$$\frac{\text{condensation rate}}{\text{maximum experimental condensation rate}}$$

The maximum experimental corrosion and condensation rates correspond to the maximum values measured for these two rates over the entire set of experimental conditions.

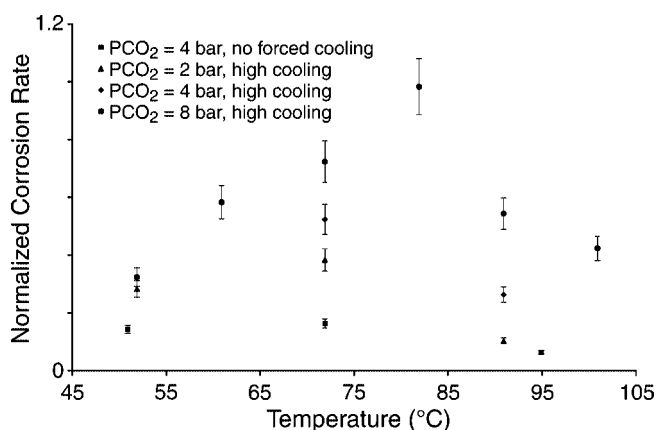


**FIGURE 3.** Influence of gas temperature on the corrosion rate at different partial pressures of CO<sub>2</sub> and different cooling rates.  $V_{\text{gas}} = 8$  m/s.

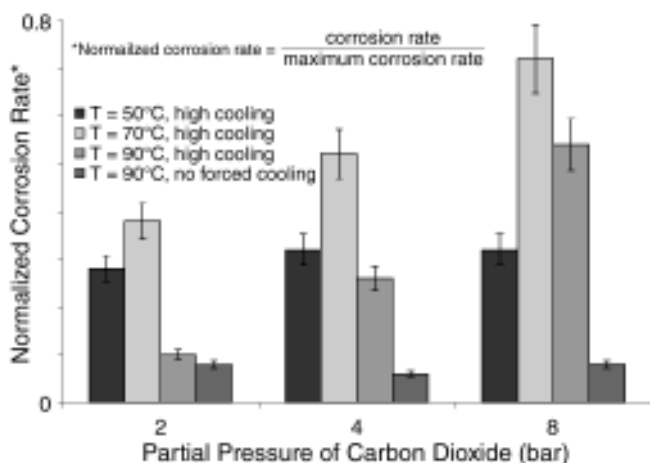


**FIGURE 4.** Influence of the partial pressure of carbon dioxide on the corrosion rate.  $V_{\text{gas}} = 8$  m/s.

These results can be interpreted as follows: at lower temperatures (<70°C), the corrosion rate increases with temperature according to Arrhenius' law applied to the endothermic reaction of corrosion by CO<sub>2</sub>. At higher temperatures (>80°C), the corrosion rate decreases as temperature increases, suggesting that an additional phenomenon occurs for such temperatures. There are at least three possible explana-

tions for this. At higher temperatures, the condensation rate is more important and the condensed liquid film at the wall is thicker. Therefore, the mass transfer of corrosive species through the condensed liquid to the wall may be limiting, which may explain a lower corrosion rate. Another explanation is that, at higher temperatures, the precipitation on the wall of the products of corrosion as an iron carbonate (FeCO<sub>3</sub>) layer may partially protect the metal from further corrosion. The third explanation may be that at higher temperatures, and thus, at higher corrosion rates, the amount of ferrous ions present in the condensed water is larger, which increases the pH of the water. The change in pH may, in turn, change the mechanism of the electrochemical reaction at the wall.<sup>5</sup> Therefore, the corresponding corrosion rate may become smaller with time. These last two assumptions are in agreement with the experimental fact that the corrosion rate should be significantly smaller at low condensation rates, as is clearly observed in Figure 3. At  $P_{\text{CO}_2} = 4$  bar and a temperature of 70°C, the corrosion rate was found to be four times higher under intense dewing conditions than the rate obtained under low condensation.

#### *Influence of the Partial Pressure of Carbon Dioxide on the Corrosion Rate*

The influence of  $P_{\text{CO}_2}$  was studied over a range from 1 bar to 8 bars at bulk temperatures of 50, 70, and 90°C and at low and high condensation rates. The experimental results regarding the corrosion rate are plotted in Figure 4. It can be seen that the partial pressure had little influence on the corrosion rate, both at 50°C with cooling and at 90°C without cooling. On the other hand, at 70°C and at 90°C with high cooling, the influence of the partial pressure of carbon dioxide was more significant. As  $P_{\text{CO}_2}$  doubled, the corrosion rate increased 40% at 70°C and more than 110% at 90°C. Comparatively, de Waard's correlation<sup>6</sup> predicts a 60% increase as the partial pressure of carbon dioxide doubles. It appears from our experimental data that the corrosion rate was sensitive to a change in  $P_{\text{CO}_2}$  at high condensation rates but was insensitive to such a change at low condensation rates. At low condensation rates, it may be easier to saturate, or even supersaturate, the condensed liquid with the products of corrosion, thus increasing the pH, and somehow, slowing down the kinetics of the reaction of corrosion by CO<sub>2</sub>. At higher condensation rates, the buffering of the pH of the solution by ferrous ions may be insignificant and the pH might be more sensitive to the change in partial pressure of carbon dioxide.

#### *Influence of the Gas Velocity on the Corrosion Rate*

The influence of gas velocity on the corrosion was studied over a range from 2 m/s to 8 m/s. It was

studied both at 90°C and 50°C. At high temperatures, the stabilized corrosion rate did not seem to be affected significantly by the change of gas velocity. On the other hand, a sudden change of the corrosion rate was observed at 50°C as the gas velocity dropped from 4 m/s to 2 m/s.

It appears that the gas velocity does not have a direct effect on the corrosion rate, but rather on the condensation rate, which, in turn, may have affected the corrosion rate. This is clearly demonstrated by Figure 5 where both the condensation rate and the corrosion rate are reported as a function of the gas velocity: at 90°C as well as at 50°C, the condensation rate decreased significantly as the gas velocity varied from 8 m/s to 2 m/s. Mass transfer in the gas phase was less important for a less turbulent flow (low velocities). Therefore, less water is available for condensation at the wall and less heat was removed, preventing the phase change of the water vapor. Meanwhile, the corrosion rate remained unaffected by a change of gas velocity, except when this change lowered the condensation rate below a critical value.

#### Influence of the Condensation Rate on the Corrosion Rate

From this experimental study, it appears that the condensation rate is dependent on all other primary parameters without exception. This complex dependence is discussed elsewhere.<sup>3</sup> This renders the prediction of the condensation rate difficult. However, it appears from the previously reported experimental data that the role of the condensation rate is central in the determination of the corrosion rate during TLC.<sup>7</sup> Therefore, its influence on the corrosion rate is studied last. In the previous paragraph, it was reported that it is in the lower range of condensation rates that a significant influence on the corrosion rate can be observed. Thus, the influence of the condensation rate was studied at 50°C, where lower condensation rates were obtained with the experimental setup previously described. It was made possible to change the condensation rate of an order of magnitude, only by changing the temperature of the pipewall by a few degrees. Results show that the corrosion rate significantly increased as the condensation rate crossed a threshold. Below this threshold, the corrosion rate measured by the ER probe initially stabilized at a comparatively lower value (Figure 6). Above the threshold, the corrosion rate stabilized at higher values. The concept of a critical threshold for the condensation rate is in agreement with the theory of a corrosion rate controlled by the level of supersaturation of the condensed water by the products of corrosion. At high condensation rates, the bulk of the condensed water may never get saturated. In this case, the corrosion rate would not be significantly dependent on the condensation rate, since no significant increase of the ferrous ion concentration is pos-

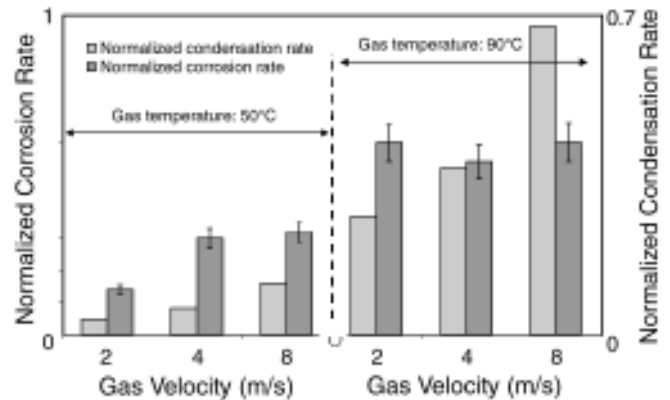


FIGURE 5. Influence of the gas velocity on the condensation rate and on the corrosion rate. High cooling,  $P_{CO_2} = 8$  bar.

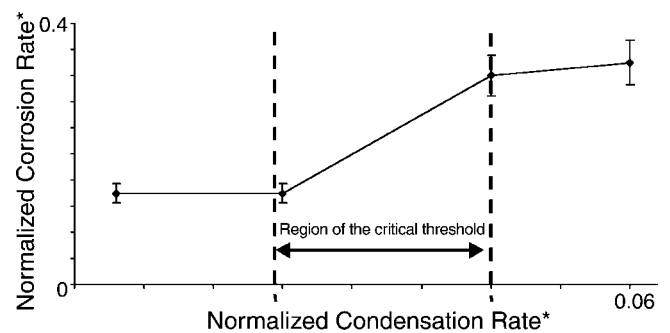


FIGURE 6. Influence of the condensation rate on the corrosion rate.  $T_{bulk} = 51^\circ\text{C} (\pm 1^\circ\text{C})$ ,  $P_{CO_2} = 4$  bar,  $V_{gas} = 8$  m/s.

sible, and therefore, no significant change in pH can occur. At low condensation rates, the water is more likely to become supersaturated with the products of corrosion. In this case, the corrosion rate would be affected by a higher pH and a lower availability of corrosive species in solution. If the temperature is high enough, the formation of a scale of  $\text{FeCO}_3$  may be possible, which could further decrease the corrosion rate. In between these two regimes of corrosion, a transition regime may exist, where the pH of condensed water changes rapidly with small perturbations of the primary parameters. Therefore, the sensitivity of the corrosion rate to the condensation rate, the wall temperature, and  $P_{CO_2}$  would be greater. This theory may explain the sudden jumps in the corrosion rate observed during a slight change of the condensation rate around the critical threshold.

#### Surface Analysis on the Coupons

The observation of the coupons after 48-h experimentations confirms the hypothesis of the formation of an  $\text{FeCO}_3$  scale, preferentially at higher temperatures and under low condensation. X-ray diffraction spectroscopy was used to identify the deposited compound. Under metallurgical microscope, the scale appeared to be sparsely deposited on the

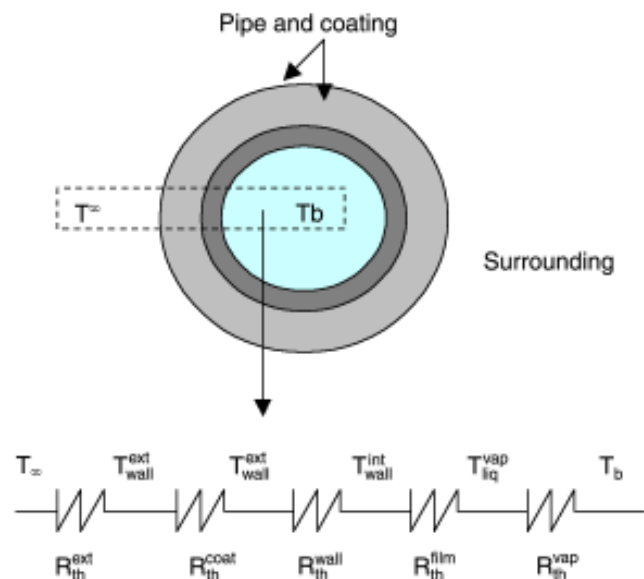


FIGURE 7. Equivalent circuit of heat-transfer resistances for a pipeline and its surrounding.

exposed surface of the coupon at 50°C. At 70°C, the scale was more uniformly deposited over the surface but clearly less dense than at 90°C. Even at 90°C, the surface showed islands of denser deposited scale (black areas) surrounded by more porous areas (gray areas).

## MODELING OF THE CORROSION RATE

To predict the corrosion rate during TLC as a function of the internal parameters and the heat exchanges with the surrounding, a better insight into the fundamental phenomena involved during corrosion under condensing conditions is needed. In particular, the condensation rate needs to be predicted before any prediction can be made of the corrosion rate.

### Modeling of the Condensation Rate of Water Vapor

The heat and mass transfer between the gas bulk and the wall can be modeled by an equivalent circuit of heat- and mass-transfer resistances as shown in Figure 7. Each of these resistances must be determined to obtain the condensation rate at the wall:

- The heat- and mass-transfer resistances in the gas phase are obtained from Dittus and Boelter's correlation for full pipe flow<sup>8</sup> adapted to the special case of low condensation at the wall.<sup>9</sup>
- The heat- and mass-transfer resistances in the condensed liquid derive from Nusselt's theory<sup>10</sup> of filmwise condensation adapted to the cylindrical geometry of a pipe.<sup>2</sup>

- The heat-transfer resistance of the pipewall and its coating are usually known from the suppliers.
- The correlation giving the external heat-transfer resistance for the specific case of a double-pipe countercurrent heat exchanger is found in the literature.<sup>8,11</sup> In the field case, the external conditions surrounding the pipeline may vary greatly from one line to another and so do the corresponding external heat-transfer resistances.

This model has proven its ability to predict accurately the condensation rate of water vapor in horizontal pipelines as well as the condensed film thickness on the inner wall of the pipe.<sup>3</sup> The model takes into consideration the influence of the bulk temperature, the total and partial pressures, the cooling rate, and the gas velocity. It is important to mention that the calculated condensed film thickness is valid only under the assumptions made in Nusselt's theory.<sup>10</sup> One of them is that only gravity and shear forces influence the hydrodynamics of the condensed liquid. This assumption is clearly not satisfied at the very top of the line (at an angle of  $\pm 10^\circ$  from the vertical line). At this specific location, surface tension and gravity forces govern the hydrodynamics of the condensed liquid and the thickness of the film is calculated differently (Equation [1]). It must be mentioned that, under the assumption of linear temperature profile in the condensed film, the condensation rate is not significantly affected by the method of computation of the film thickness: in both cases, the corresponding heat-transfer resistances in the condensed liquid film are significantly smaller than the heat-transfer resistance occurring in the gas phase.

### Modeling the Corrosion Rate during TLC

During this study, the influence of three main phenomena occurring during TLC was modeled, and the results of simulation were tested against experimental data:

- influence of mass transfer of corrosive species through the condensed liquid film to the wall
- change of chemistry in the condensed liquid at the top of the line and the corresponding change in pH
- influence of the formation of a corrosion product layer on the wall

### Influence of the Mass Transfer in the Condensed Liquid

In the case of filmwise condensation, a two-dimensional, transient, computational fluid dynamic code was developed,<sup>3</sup> solving the mass transfer of corrosive species in the condensed liquid film with the following boundary conditions:

- Vapor-liquid thermodynamic equilibrium at the gas-condensed liquid interface
- Flux of consumption of species at the wall according to the kinetics of the electrochemical reaction involved. The corrosion rate can be obtained either from the semi-empirical model developed by de Waard and Lotz<sup>6</sup> or by the mechanistic model developed by Nešić, et al.<sup>5</sup>

Both convective and diffusive fluxes in the condensed liquid were solved. Results show that, for a film thickness of 20 mm to 100 mm (common range during filmwise condensation), the corrosion rate obtained at steady state moderately decreased as the condensed liquid film thickness increased, mainly due to a limitation in mass transfer of corrosive species to the wall. These results are in agreement with the previous theoretical<sup>12</sup> and experimental<sup>13</sup> work published on atmospheric corrosion. Such a model also showed that under filmwise condensation, the concentration of ferrous ions in the condensed water was never higher than a few ppm, even at the surface of the wall. Therefore, no saturation of the condensed water with ferrous ions and no precipitation of  $\text{FeCO}_3$  could occur under flowing conditions.<sup>3</sup>

Assuming that, at the top of the line, the surface tension force determines the hydrodynamics of the film, the average film thickness on the underside vertical surface of the inner pipewall is:<sup>14</sup>

$$\delta = \left[ \frac{\sigma}{g \times (\rho_l - \rho_g)} \right]^{1/2} \quad (1)$$

$\sigma$  is the surface tension coefficient,  $g$  is the gravity constant,  $\rho_l$  is the liquid density, and  $\rho_g$  is the gas density. Figure 8 shows that the corrosion rate obtained at steady state was then significantly dependent on the film thickness. This is explained by the absence of convective mass transfer as well as an increased film thickness, which renders diffusion of corrosive species to the wall a limiting step.

### Influence of the Change in Chemistry of the Condensed Water

From this point forward, the model presented applies to the case where surface tension forces determine the shape of the film and the accumulation of products of corrosion is possible. During the reaction of corrosion, ferrous ions are produced and released into the condensed water. At any time, the pH of the solution can be obtained by simultaneously solving the equation of the thermodynamic equilibrium between the gas phase and the liquid phase, the equation of dissolution of  $\text{CO}_2$ , the equation of electroneutrality, and the equations of dissociation of carbonic acid ( $\text{H}_2\text{CO}_3$ ):

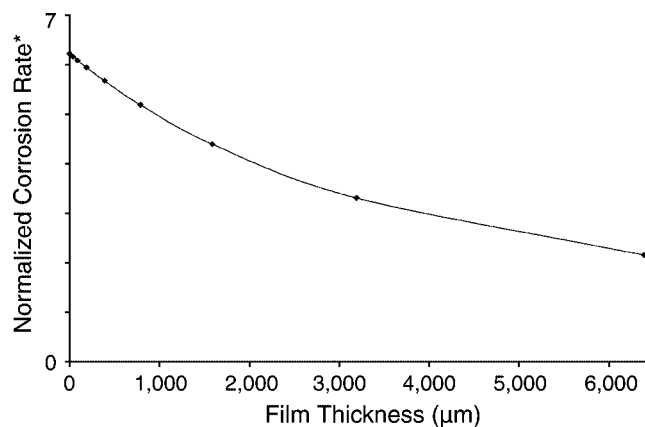


FIGURE 8. Simulated corrosion rate as a function of film thickness for stagnant condensed water (no convection).  $T = 90^\circ\text{C}$ ,  $P_{\text{CO}_2} = 4 \text{ bar}$ .

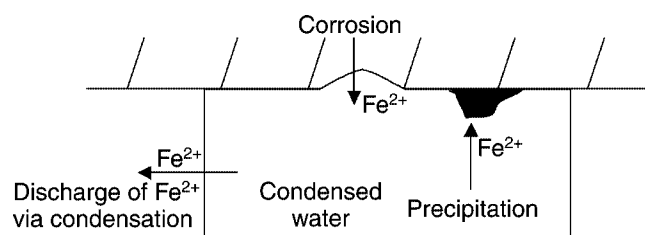
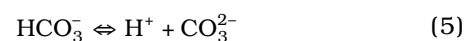


FIGURE 9. Transport, source, and sink of iron ions during TLC.



$$\sum_{i=1}^N z_i c_i = 0 \quad (6)$$

The value of the equilibrium constants corresponding to these reactions are given elsewhere.<sup>5</sup> Additionally, if the saturation of the water is reached, these ferrous ions combine with carbonate ions to form  $\text{FeCO}_3$ :



$\text{FeCO}_3$  is a solid that deposits on the surface of the pipe. Under certain conditions to be determined, the deposited layer can protect the metallic wall from further corrosion. Figure 9 represents a control volume of condensed water attached to the pipewall. The transport, source, and sink of ferrous ions in this condensed water are also pictured. A material balance applied to the condensed water gives:

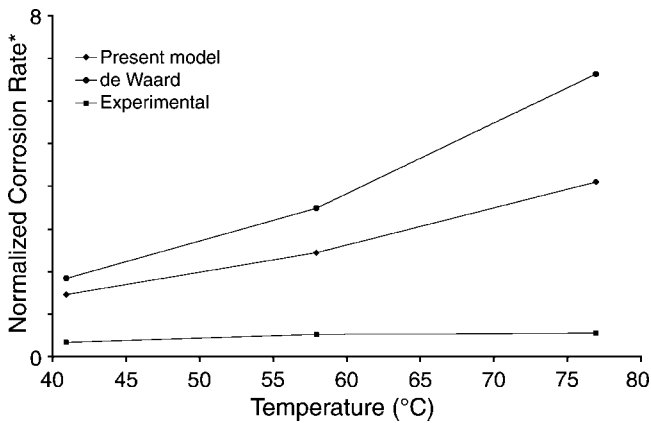


FIGURE 10. Comparison of the experimental and theoretical corrosion rates. Influence of temperature.  $P_{CO_2} = 8$  bar.

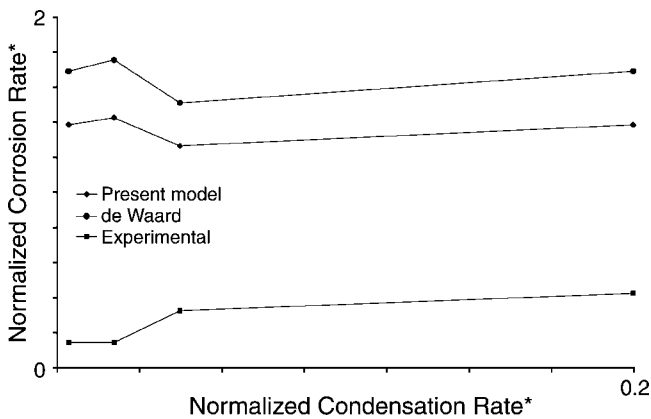


FIGURE 12. Comparison of the experimental and theoretical corrosion rates. Influence of the condensation rate.  $T_{gas} = 50^\circ C$ ,  $P_{CO_2} = 4$  bar.

$$\frac{d(V \times [Fe^{2+}])}{dt} = \Phi_c \times A_c - \Phi_p \times A_p - \dot{m} \times A_{cond} \times [Fe^{2+}] \quad (8)$$

$V$  is volume of condensed water ( $m^3$ ),  $[Fe^{2+}]$  is concentration of ferrous ions in solution ( $kmol/m^3$ ),  $\Phi_c$  is corrosion rate ( $kmol/m^2/s$ ),  $A_c$  is the area where corrosion takes place ( $m^2$ ),  $\Phi_p$  is precipitation rate ( $kmol/m^2/s$ ),  $A_p$  is the area where precipitation takes place ( $m^2$ ),  $\dot{m}$  is condensation rate ( $m^3/m^2/s$ ), and  $A_{cond}$  is the area where condensation takes place ( $m^2$ ). If one assumes that the area of corrosion, precipitation, and condensation are equal and if it is further assumed that the condensed film thickness,  $\delta$ , is known, Equation (8) becomes:

$$\frac{d([Fe^{2+}])}{dt} = \frac{1}{\delta} \times [\Phi_c - \Phi_p - \dot{m} \times [Fe^{2+}]] \quad (9)$$

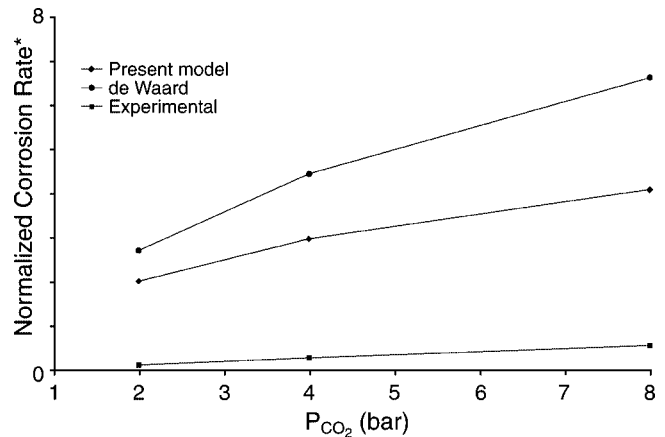


FIGURE 11. Comparison of the experimental and theoretical corrosion rates. Influence of the partial pressure of carbon dioxide.  $T_{gas} = 80^\circ C$ .

In absence of a protective scale on the steel surface, the corrosion rate,  $\Phi_c$ , is determined according to the electrochemical model developed by Nešić, et al.<sup>5</sup> The condensation rate is determined according to the model presented earlier in this paper. The precipitation rate is calculated as suggested by Van Hunnik.<sup>15</sup> Equation (9) can be discretized in time as follows:

$$[Fe^{2+}]_{t+\Delta t} = [Fe^{2+}]_t + \frac{\Delta t}{\delta} \times [\Phi_c(t) - \Phi_p(t) - \dot{m} \times [Fe^{2+}]_t] \quad (10)$$

The computational procedure, which solves Equations (2) through (6) and (10) simultaneously, determines the change in pH and the ferrous ion concentration with time. The corresponding corrosion rate was calculated and allowed for the prediction of the new concentration of ferrous ions at the next time step. The iteration was continued until no additional change in the ferrous ion concentration was computed.

Experimental and theoretical corrosion rates, as well as the corrosion rate according to de Waard's model (presently modified to take into consideration the mass transfer in the condensed film as described previously), are also plotted against the temperature, the partial pressure, and the condensation rate in Figures 10 through 12, respectively. In general, the corrosion rate was overpredicted by both of the models. Moreover, the present model showed an increase in the corrosion rate as the temperature increased above  $80^\circ C$  whereas the experimental corrosion rate decreased above such temperature. The overprediction of the corrosion rate is due to the fact that further protection of the depositing  $FeCO_3$  scale on the

metal is not taken into consideration. According to the present model, the influence of the temperature on the corrosion rate at low condensation rate is predominant. Experimentally, as the normalized condensation rate\* increased from 0.02 to 0.03, the corresponding wall temperature decreased from 52°C to 48°C. Accordingly, the predicted normalized corrosion rate\* decreased from 1.42 to 1.26. Experimentally, an increase in the corrosion rate from 0.14 to 0.32 was observed, suggesting that at low condensation rates, the influence of the condensation rate on the corrosion rate was predominant rather than the influence of temperature. It appears that the sensitivity of the model to the change in condensation rate is not sufficient. Clearly, neither the influence of the hydrodynamics nor the influence of the chemistry of the condensed water is sufficient to predict the corrosion rate during TLC.

\*Normalized condensation rate =

$$\frac{\text{condensation rate}}{\text{maximum experimental condensation rate}}$$

\*Normalized corrosion rate =

$$\frac{\text{corrosion rate}}{\text{maximum experimental corrosion rate}}$$

Even if the prediction of the corrosion rate was less conservative when the saturation of the condensed water by-products of corrosion was taken into consideration, the theoretical results still overpredicted the experimental ones by 1 order of magnitude. Therefore, the formation of a scale that deposits on the metal surface and partially protects it from further corrosion is necessary. An approach for the modeling of the influence of an  $\text{FeCO}_3$  scale on the corrosion rate is developed in what follows.

### Influence of the Deposition of an Iron Carbonate Scale

The role of a protective scale can be grossly simplified by considering that part of the corroding surface is now covered by the products of corrosion and, on a covered site, no further corrosion occurs. On the uncovered surface, only corrosion occurs. If one considers that the scale covers a percentage  $(1-K)$  of the corroding surface,  $K$  being greater than or equal to 0 and smaller than or equal to 1, the material balance presented in Equation (2) becomes:

$$\frac{d([\text{Fe}^{2+}])}{dt} = \frac{1}{\delta} \times \left[ K \times \Phi_c - (1-K) \times \Phi_p - \dot{m} \times [\text{Fe}^{2+}] \right] \quad (11)$$

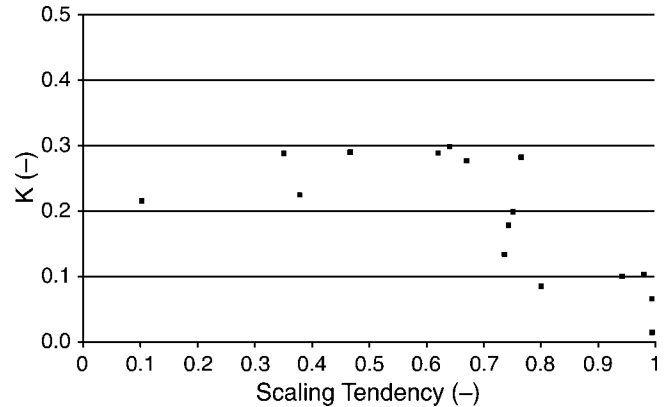


FIGURE 13. Factor  $K$  ( $1-K$  representing the surface coverage) as a function of the scaling tendency.

The discretized form of this equation is:

$$[\text{Fe}^{2+}]_{t+\Delta t} = [\text{Fe}^{2+}]_t + \frac{\Delta t}{\delta} \times \left[ K \times \Phi_c(t) - (1-K) \times \Phi_p(t) - \dot{m} \times [\text{Fe}^{2+}]_t \right] \quad (12)$$

Following the same computational procedure as the one developed for the prediction of the corrosion rate in absence of a protective scale but using Equation (12) rather than Equation (10), the chemistry of the water during scaling conditions was derived in time. The iterative computation of the ferrous ion concentration converged to give the corrosion rate at steady state in the presence of a protective scale.

The surface coverage  $(1-K)$  was determined by tuning the mechanistic model developed here so that it fit the experimental corrosion rates obtained from 17 experiments run over a wide range of temperatures,  $P_{\text{CO}_2}$ , and condensation rates.  $K$  is plotted as a function of the scaling tendency in Figure 13. The scaling tendency is defined as the ratio of the precipitation rate (in  $\text{kmol/m}^2/\text{s}$ ; as calculated in Reference 15) to the corrosion rate in absence of a scale<sup>7</sup> (in  $\text{kmol/m}^2/\text{s}$ ) as given by the present model. From Figure 13, it can be seen that the results are distributed in a stepwise manner. Below a scaling tendency of 0.7,  $K$  remained almost constant and within a range from 0.2 to 0.3. Above a scaling tendency of 0.7 and up to 0.99,  $K$  dropped to a stable value around 0.1. Above a scaling tendency of 0.99,  $K$  decreased quickly to values as low as 0.01.

The observed results are in agreement with the ones published by Pots and Hendriksen<sup>7</sup> in the sense that the protectiveness of a scale seems to correlate well with the scaling tendency. Pots reports a critical scaling tendency of 0.5 for a scale to become protective. In the case of TLC, the protectiveness of the scale is related in a stepwise manner to the scaling

tendency, corresponding to different "levels of coverage" of the surface. For a scaling tendency close to 1, the coverage is almost total. For a scaling tendency <0.7, the coverage is ~70% of the corroding surface.

## CONCLUSIONS

❖ A model has been developed that gives a better insight into the mechanisms involved during TLC. In particular, the influence of the mass transfer in the condensed liquid film, saturation of the condensed liquid with the products of corrosion, and formation of an  $\text{FeCO}_3$  scale have been studied. A full-scale flow-loop for TLC experimentation has been designed at the Institute for Corrosion and Multiphase Technology and a new generation of corrosion probes has been selected and validated to obtain experimental corrosion rates during TLC. Even if they play a role in the determination of the corrosion rate, neither the mass transfer nor the chemistry of the condensed water can completely explain the experimental data obtained at the Institute for Corrosion and Multiphase Technology. By introducing the surface coverage to take into consideration the influence of a deposited  $\text{FeCO}_3$  scale, it is possible to tune the mechanistic model with the experimental data. The surface coverage can then be correlated with the scaling tendency. The surface coverage is found to correlate in a stepwise manner with the scaling tendency.

## REFERENCES

1. M. Estavoyer, "Corrosion Problems at Lack Sour Gas Field," *H<sub>2</sub>S Corrosion in Oil and Gas Production* (Houston, TX: NACE International, 1981), p. 905.
2. F. Vitse, K. Alam, Y. Gunaltun, D. Larrey de Torreben, P. Duchet-Suchaux, "Semi-Empirical Model for Prediction of the Top-of-the-Line Corrosion Risk," *CORROSION/2002*, paper no. 245 (Houston, TX: NACE, 2002).
3. F. Vitse, "Experimental and Theoretical Study of the Phenomena of Corrosion by Carbon Dioxide under Dewing Conditions at the Top of a Horizontal Pipeline in Presence of a Noncompensable Gas" (PhD diss., Ohio University, 2002).
4. B. Hemblade, Ceion Technology User's Manual, <http://www.cormon.com>, 2001.
5. S. Nešić, J. Postlethwaite, S. Olsen, "An Electrochemical Model for Prediction of CO<sub>2</sub> Corrosion," *CORROSION/95*, paper no. 131 (Houston, TX: NACE, 1995).
6. C. De Waard, U. Lotz, "Prediction of CO<sub>2</sub> Corrosion of Carbon Steel," *CORROSION/93*, paper no. 69 (Houston, TX: NACE, 1993).
7. B.F.M. Pots, E.L.J.A. Hendriksen, "CO<sub>2</sub> Corrosion under Scaling Conditions—The Special Case of Top-of-Line Corrosion in Wet Gas Pipelines," *CORROSION/2000*, paper no. 31 (Houston, TX: NACE, 2000).
8. F.W. Dittus, L.M.K. Boetler, *Univ. Calif. (Berkeley) Pub. Eng.* 2 (1930): p. 443.
9. K. Stephan, A. Laesecke, *Warme-u. Stoffubertrag.* 13 (1980): p. 115-123.
10. W. Nusselt, *VDI-Z* 60 (1916): pp. 441-546, 569-575.
11. X. Chen, P. Hawkins, D. Solberg, *Trans. Am. Soc. Eng.* 68 (1946): p. 99.
12. N.D. Tomashov, *Corrosion* 20 (1964): p. 7t.
13. A. Nishikata, Y. Ichihara, Y. Hayashi, T. Tsuru, *J. Electrochem. Soc.* 144, 4 (1997): p. 1,244-1,252.
14. J. Gerstmann, P. Griffith, *Int. J. Heat Mass Transf.* 10 (1967): p. 567-580.
15. E.W.J. Van Hunnik, "The Formation of Protective  $\text{FeCO}_3$  Corrosion Product Layers in CO<sub>2</sub> Corrosion," *CORROSION/96*, paper no. 6 (Houston, TX: NACE, 1996).

**Need  
reprints  
of  
CORROSION  
ads,  
articles,  
or  
covers?**

THE JOURNAL OF SCIENCE AND ENGINEERING  
**CORROSION**

## REPRINTS ARE A GREAT INVESTMENT!

- ❖ Increase your company's exposure at trade shows and conferences
- ❖ Promote your company's products and services
- ❖ Generate sales through direct mail campaigns and sales calls
- ❖ Promote your professional image as an industry expert
- ❖ Educate employees and colleagues on the latest industry trends and technology
- ❖ And much more!



Professionally printed reprints and photocopied reprints are available of all *CORROSION* ads, articles, and covers. Reprints can be customized with your company's logo, additional product information, or the magazine cover—with no limits on creativity!

Order your reprints today, it simply makes good business sense!  
For reprint information and rates, call 281/228-6219.